Top Quark Forward-Backward Asymmetry in e^+e^- Annihilation at Next-to-Next-to-Leading Order in QCD

Jun Gao[1,2,*] and Hua Xing Zhu[3,†]
[1]Department of Physics, Southern Methodist University, Dallas, Texas 75275-0175, USA
[2]High Energy Physics Division, Argonne National Laboratory, Argonne, Illinois 60439, USA
[3]SLAC National Accelerator Laboratory, Stanford University, Stanford, California 94309, USA
(Received 20 October 2014; published 31 December 2014)

We report on a complete calculation of electroweak production of top-quark pairs in e^+e^- annihilation at next-to-next-to-leading order in quantum chromodynamics. Our setup is fully differential in phase space and can be used to calculate any infrared-safe observable. Especially we calculated the next-to-next-to-leading-order corrections to the top-quark forward-backward asymmetry and found sizable effects. Our results show a large reduction of the theoretical uncertainties in predictions of the forward-backward asymmetry, and allow for a precision determination of the top-quark electroweak couplings at future e^+e^- colliders.

DOI: 10.1103/PhysRevLett.113.262001 PACS numbers: 12.38.Bx, 12.60.-i, 14.65.Ha

Introduction.—Top-antitop quark pairs can be copiously produced at future International Linear Collider (ILC), facilitating a detailed study of top-quark properties [1]. The clean environment of a lepton collider allows measurement of the process $e^+e^- \to t\bar{t}$ to very high accuracy, which also demands high precision in theoretical calculation, in particular the inclusion of higher order QCD radiative corrections. In the past, significant theoretical efforts have been focused on $t\bar{t}$ production at threshold, for which the next-to-next-to-leading-order (NNLO) QCD corrections are known for more than a decade [2], and even the next-to-next-to-next-to-leading order QCD corrections will be available in the near future [3]. However, for $t\bar{t}$ production in the continuum, only the total cross section is known in the high-energy expansion [4]. Ingredients for a fully differential NNLO calculation in the continuum have been obtained by different groups [5,6]. Recently, we reported a fully differential NNLO calculation for the photon-mediated contributions [7], using a NNLO generalization of a phase space slicing method [8,9]. In this Letter, we complete this calculation by including also the standard model (SM) Z boson contributions. Independently, calculation of inclusive cross section for $e^+e^- \to \gamma^* \to t\bar{t}$ at NNLO based on massive generalization of the antenna subtraction method [10] has been reported recently in Ref. [11].

As an important application of our results, we consider the calculation of top-quark forward-backward (FB) asymmetry ($A_{\rm FB}$) at NNLO in e^+e^- collision in the continuum. In the limit of small top quark mass, this observable has been computed to NNLO in Refs. [12]. The full mass effect is only known for the pure two-loop virtual contributions [13]. In this Letter, we report the first calculation of this observable at NNLO in QCD, including both loop and real-radiation contributions. $A_{\rm FB}$ is an important precision observable for the determination of neutral-current electroweak couplings of top quark to photon and Z boson. Their precise measurement is an important probe of physics beyond the SM, such as Randall-Sundrum models [14], and models of compositeness [15]. Information of top-quark neutral coupling is encoded in the top-quark form factor. For an on-shell $t\bar{t}$ pair, the form factor can be expressed by four independent scalar ones,

$$\Gamma_\mu^{ttV}(Q_\mu) = -ie\left[\gamma_\mu\left(F_{1v}^V(Q^2)+\gamma_5 F_{1a}^V(Q^2)\right) + \left(\frac{\sigma_{\mu\nu}}{2m_t}Q^\nu\left(iF_{2v}^V(Q^2)+\gamma_5 F_{2a}^V(Q^2)\right)\right)\right], \quad (1)$$

where Q_μ is the total four-momentum of $t\bar{t}$, e is the positron charge, and m_t is the top-quark mass. V denotes photon (γ) or Z boson. To leading order (LO) in electroweak theory and QCD, the vector and axial form factors, $F_{1v}^V(Q^2)$ and $F_{1a}^V(Q^2)$, are given by

$$F_{1v}^\gamma = Q_t, \qquad F_{1a}^\gamma = 0,$$
$$F_{1v}^Z = \frac{1}{\sin 2\vartheta}\left(\frac{1}{2}-2Q_t\sin^2\vartheta\right), \qquad F_{1a}^Z = \frac{-1}{2\sin 2\vartheta}. \quad (2)$$

$Q_t = 2/3$ is the top-quark charge in unit of e, and ϑ is the weak-mixing angle. At ILC the top-quark forward-backward asymmetry can be measured to a precision of around 1%, in both the fully hadronic or semileptonic channels [16–18], far beyond the precision the LHC can reach [17]. It thus provides strong sensitivity to any new physics that could modify the top-quark electroweak couplings. In this Letter, we computed the fully differential NNLO QCD corrections to the exclusive production of top-quark pairs and thereby obtain the $A_{\rm FB}$ at NNLO for the first time. Our calculation provides the most precise QCD predictions on $A_{\rm FB}$ including its theoretical uncertainties, and also allows corrections

for experimental acceptance using the full kinematic information.

The formalism.—A fully differential calculation for $e^+e^- \to t\bar{t}$ at NNLO in QCD involves three types of diagrams, namely the two-loop virtual diagrams, one-loop real-virtual diagrams, and double real-emission diagrams. The individual contributions of these diagrams have been known for some time. However, combining them in a consistent way is a nontrivial task due to the presence of infrared singularities in QCD matrix elements. To this end, we employ a NNLO generalization of phase-space slicing method, described in detail in a previous publication [7]. We briefly summarize its essential features here.

In perturbative QCD, differential cross section for any infrared-safe observable O has a schematic form

$$\frac{d\sigma}{dO} = \int dPS_{t\bar{t}+X} |\mathcal{M}_{e^+e^-\to t\bar{t}X}|^2 \delta[O - F(\{p_i\})], \quad (3)$$

where O is calculated from the final-state momentum $\{p_i\}$ through measurement function F. Inserting a unit decomposition $1 = \Theta(\lambda - E_X) + \Theta(E_X - \lambda) \equiv \Theta_{\rm I} + \Theta_{\rm II}$, we can write Eq. (3) as

$$\frac{d\sigma}{dO} = \frac{d\sigma_{\rm I}}{dO} + \frac{d\sigma_{\rm II}}{dO}, \quad (4)$$

where

$$\frac{d\sigma_{\rm I}}{dO} = \int dPS_{t\bar{t}+X} |\mathcal{M}_{e^+e^-\to t\bar{t}X}|^2 \delta[O - F(\{p_i\})]\Theta_{\rm I},$$
$$\frac{d\sigma_{\rm II}}{dO} = \int dPS_{t\bar{t}+X} |\mathcal{M}_{e^+e^-\to t\bar{t}X}|^2 \delta[O - F(\{p_i\})]\Theta_{\rm II}.$$

Obtaining $\mathcal{O}(\alpha_s^2)$ corrections to $d\sigma/dO$ simply amounts to achieving the same order of accuracy for $d\sigma_{\rm I}/dO$ and $d\sigma_{\rm II}/dO$. For $d\sigma_{\rm II}/dO$, this is simple. The presence of theta function $\Theta_{\rm II}$ implies that other than the $t\bar{t}$ pair, there is at least one parton with *finite energy* in the final state. The existence of this parton regulates the so-called double-unresolved divergences in the QCD matrix elements. The only infrared divergences (soft or collinear) left can be easily dealt with using any NLO subtraction scheme [19,20]. In other words, the $\mathcal{O}(\alpha_s^2)$ contributions to $d\sigma_{\rm II}/dO$ can be obtained from a standard NLO QCD calculation for $e^+e^- \to t\bar{t}j$ [6]. The results will exhibit logarithmic dependence on the artificial parameter λ. Our implementation of this calculation is as follows. We employ the massive version of the dipole subtraction method [20] for infrared subtraction. The one-loop real-virtual calculation is carried out by the automated program GoSam2.0 [21] with loop integral reductions performed with Ninja [22,23] and scalar integrals from OneLOop [24,25]. Note that when $\sqrt{s} > 4m_t$, the channel for production of $t\bar{t}t\bar{t}$ is open. However, these additional contributions are themselves infrared finite and small for the energy range considered here, thus they are not included. Similarly, we do not include the real emission diagrams of which γ^*/Z^* couples to light or bottom quarks and the top quarks that come from gluon splitting. Those contributions are also small, and do not contribute to the top-quark FB asymmetry.

The calculation of $d\sigma_{\rm I}/dO$ is substantially more involved. However, significant simplification can be achieved if $\lambda \ll m_t$ (we count m_t and $\sqrt{s}$, the center-of-mass energy, the same order). In that regime, universal factorization properties of QCD matrix elements allow one to write the distribution as soft-virtual (SV) contributions plus power-suppressed terms.

$$\frac{d\sigma_{\rm I}}{dO} = \frac{d\sigma_{\rm SV}}{dO} + \mathcal{O}\left(\frac{\lambda}{m_t}\right), \quad (5)$$

where a soft expansion has been performed in $d\sigma_{\rm SV}/dO$ through the phase-space volume, the matrix elements, and the measurement function. As explained in Ref. [7], the soft-virtual contributions have a factorized form of product of the hard function and soft function, each of which is known to $\mathcal{O}(\alpha_s^2)$ in analytic form. The hard function is essentially the heavy quark form factors calculated in Refs. [5], and the soft function is the phase-space integral in the eikonal limit. The soft function is the same for γ or Z mediated contributions. Comparing with the vector contributions calculated in Ref. [7], the only difference is the inclusion of axial-vector and anomaly contributions in the hard function. We note that $d\sigma_{\rm SV}/dO$ also exhibits logarithmic dependence on λ.

Combining $d\sigma_{\rm SV}/dO$ and $d\sigma_{\rm II}/dO$, we obtain a formally exact result for $d\sigma/dO$, in the limit $\lambda \to 0$. However, such a limit can never be reached because $d\sigma_{\rm II}/dO$ is usually computed numerically. In practice, we choose the parameter sufficiently small such that the power-suppressed terms can be safely neglected, and the kinematic approximation in the soft-virtual contributions can be justified. The appropriate choice of λ can be indicated by searching for a region in which the dependence on λ in $d\sigma_{\rm SV}/dO + d\sigma_{\rm II}/dO$ is minimized.

Total cross sections.—We first present our numeric results on total cross sections. We use two-loop running of the QCD coupling constant with $N_l = 5$ active quark flavors and $\alpha_s(M_Z) = 0.118$. We choose the G_F parametrization scheme [26] for the electroweak couplings with $M_W = 80.385$ GeV, $M_Z = 91.1876$ GeV, $M_t = 173$ GeV, and $G_F = 1.166379 \times 10^{-5}$ GeV^{-2} [27]. The renormalization scale is set to the center of mass energy $\sqrt{s}$ unless otherwise specified. The production cross sections through to NNLO in QCD can be expressed as

$$\sigma_{\rm NNLO} = \sigma_{\rm LO}(1 + \Delta^{(1)} + \Delta^{(2)}), \quad (6)$$

where $\Delta^{(1)}[\Delta^{(2)}]$ denotes the $\mathcal{O}(\alpha_s)[\mathcal{O}(\alpha_s^2)]$ QCD corrections. Analytic results for $\Delta^{(2)}$ are presented for production

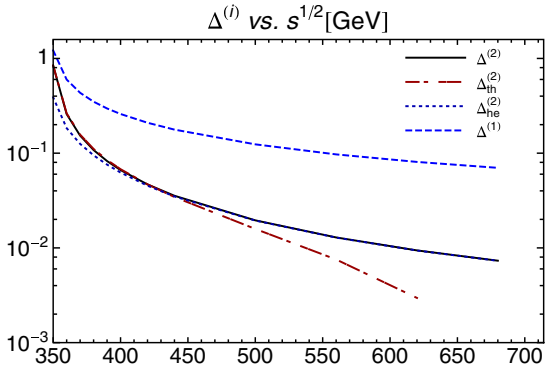

FIG. 1 (color online). Comparison of $\mathcal{O}(\alpha_s^2)$ corrections to total cross sections, $\Delta^{(2)}$, with the threshold results $\Delta_{\rm th}^{(2)}$ and high-energy expansion results $\Delta_{\rm he}^{(2)}$, as functions of the collision energy.

near threshold [2] or by high-energy expansions [4] with which we compare our numerical results.

Figure 1 shows detailed comparison of our numerical results with the threshold [2] and high-energy expansion results [4] in a wide range of collision energy. It can be seen that our full results work well in the entire energy region, i.e., approaching the threshold results at lower energies and the high-energy expansions on the other end. The $\mathcal{O}(\alpha_s^2)$ corrections can reach as large as 80% for $\sqrt{s} = 350$ GeV, due to Coulomb singularities at threshold. On the other hand, the $\mathcal{O}(\alpha_s^2)$ corrections are about 2% at intermediate collision energies and decreases rapidly to below 1% at high energies. The good agreements of our results on total cross sections with the ones from threshold and high-energy expansions in the corresponding energy region further validate our calculation.

Differential distributions and $A_{\rm FB}$.—We can calculate the fully differential distributions through to NNLO in QCD based on the phase-space slicing method. At LO, there is only one nontrivial kinematic variable, which we can choose either as cosine of the scattering angle between the final-state top quark and the initial-state electron $\cos\theta_t$, or transverse momentum of the top quark with respect to the beam-line direction $p_{T,t}$. Similar to the inclusive cross section, we can define the $\mathcal{O}(\alpha_s)$ and $\mathcal{O}(\alpha_s^2)$ corrections for each kinematic bin as $\Delta_{\rm bin}^{(1)}$ and $\Delta_{\rm bin}^{(2)}$, in analogy to Eq. (6). The results are shown in Fig. 2 for $\cos\theta_t$ and Fig. 3 for $p_{T,t}$ distributions with a typical collision energy of 400 GeV. The $\mathcal{O}(\alpha_s^2)$ corrections are about one fourth of the $\mathcal{O}(\alpha_s)$ corrections for the total cross section. However, they show a different kinematic dependence. From Fig. 2 we can see that both the $\mathcal{O}(\alpha_s)$ and $\mathcal{O}(\alpha_s^2)$ corrections are larger in the forward direction and thus will increase the FB asymmetry. Moreover, the differences of $\Delta_{\rm bin}^{(2)}$ in the forward and backward regions are of similar size as for $\Delta_{\rm bin}^{(1)}$. Thus the $\mathcal{O}(\alpha_s^2)$ corrections to $A_{\rm FB}$ are as important as the $\mathcal{O}(\alpha_s)$ corrections which will be shown later. The transverse momentum distribution in Fig. 3 shows a different feature compared to the angular distribution since the former one is

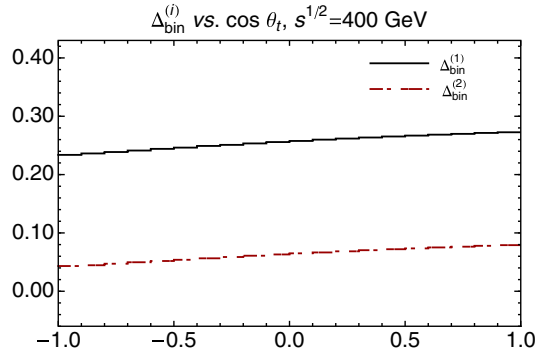

FIG. 2 (color online). $\mathcal{O}(\alpha_s)$ and $\mathcal{O}(\alpha_s^2)$ corrections in different $\cos\theta$ bins of top quark, $\Delta_{\rm bin}^{(1)}$ and $\Delta_{\rm bin}^{(2)}$, for $\sqrt{s} = 400$ GeV.

also affected by the energy spectrum of the top quark. The real corrections pull the energy spectrum to the lower end and thus the $p_{T,t}$ distribution as well. As shown in Fig. 3, the $\mathcal{O}(\alpha_s^2)$ corrections are positive in the low p_T region and decrease to negative values near the kinematic limits. The $\mathcal{O}(\alpha_s^2)$ corrections show a relatively larger impact in the $p_{T,t}$ distribution.

The forward-backward asymmetry $A_{\rm FB}$ is defined as the number of top quarks observed in the forward direction minus the one observed in the backward direction, divided by the total number of top quark observed,

$$A_{\rm FB} = \frac{\sigma_A}{\sigma_S} \equiv \frac{\sigma(\cos\theta_t > 0) - \sigma(\cos\theta_t < 0)}{\sigma(\cos\theta_t > 0) + \sigma(\cos\theta_t < 0)}, \qquad (7)$$

We show $A_{\rm FB}$ at LO as a function of the collision energy in the lower inset of Fig. 4. The $A_{\rm FB}$ at NLO and NNLO are calculated by using the corresponding NLO and NNLO cross sections in both the denominator and numerator of Eq. (7), and are shown in the upper inset of Fig. 4. All curves are normalized to the $A_{\rm FB}$ at LO. The $\mathcal{O}(\alpha_s)$ corrections are about 2% for $\sqrt{s}$ around 500 GeV. The $\mathcal{O}(\alpha_s^2)$ corrections further increase $A_{\rm FB}$ by about 1.2% for the same region. We also plot the $A_{\rm FB}$ calculated using the two-loop threshold cross sections [13] for comparison,

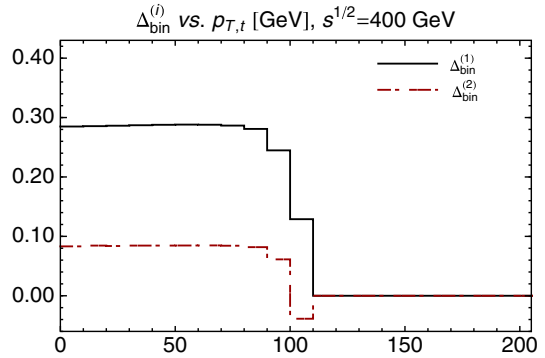

FIG. 3 (color online). $\mathcal{O}(\alpha_s)$ and $\mathcal{O}(\alpha_s^2)$ corrections in different p_T bins of top quark, $\Delta_{\rm bin}^{(1)}$ and $\Delta_{\rm bin}^{(2)}$, for $\sqrt{s} = 400$ GeV.

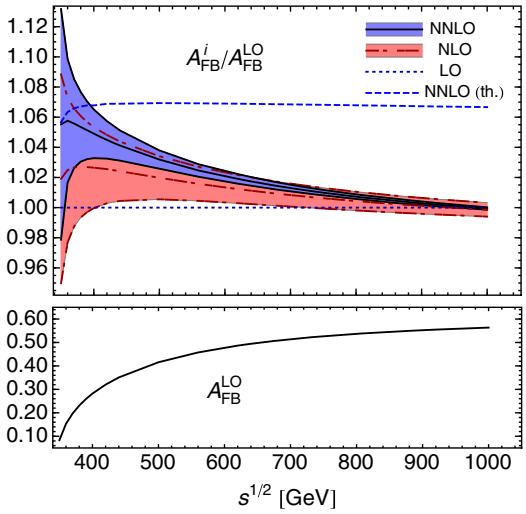

FIG. 4 (color online). Lower inset: top-quark A_{FB} at the LO as a function of collision energy; upper inset: ratios of A_{FB} at the NLO and NNLO to A_{FB} at the LO. The threshold approximation is denoted as th.

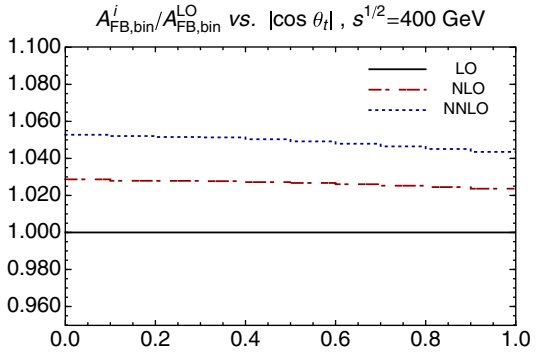

FIG. 5 (color online). Top-quark forward-backward asymmetry in different $|\cos\theta_t|$ bins, $A_{FB,bin}$, normalized to the LO predictions, for $\sqrt{s} = 400$ GeV.

which shows good agreement with our exact result in the energy region just above the production threshold. This is expected since in the threshold region the former ones dominate. We further investigate uncertainties of predictions on A_{FB} due to missing corrections beyond NNLO. A conventional way to estimate those uncertainties is by checking the residual QCD scale dependence. However, for ratios like A_{FB}, if we vary the scales simultaneously in σ_A and σ_S, it tends to underestimate the uncertainty. For example, the NLO prediction with scale uncertainty does not overlap with the NNLO prediction. Thus a more appropriate prescription is to vary the scales independently in σ_A and σ_S. We change the scale by a factor of two upward and downward in both σ_A and σ_S, and add their fractional uncertainties to A_{FB} in quadrature. The predicted uncertainties are shown in Fig. 4 by colored bands. With the $\mathcal{O}(\alpha_s^2)$ corrections, the scale uncertainty on A_{FB} has been reduced to less than half of the value at NLO as further shown in Table. I. The third and fourth columns in Table I show the NLO and NNLO predictions of A_{FB} together with the scale uncertainties, all shown in percentage. The column δA_{FB}^{NNLO} presents variation of FB asymmetry due to uncertainty of top-quark mass input, which is taken to be ± 0.5 GeV for comparison. For a typical collision energy of 500 GeV, the residual scale uncertainty of NNLO prediction on A_{FB} is 0.0025, which is well below the projected experimental precision of the future ILC [16]. The uncertainty due to top-quark mass input is relatively small especially considering the projected precision on mass measurement at the ILC.

TABLE I. Top-quark forward-backward asymmetry at different perturbative orders for representative $\sqrt{s}$ choices. The FB asymmetries are shown in percentage.

$\sqrt{s}$ (GeV)	A_{FB}^{LO}	A_{FB}^{NLO}	A_{FB}^{NNLO}	δA_{FB}^{NNLO}
400	28.20	28.94 ± 0.76	29.58 ± 0.46	± 0.26
500	41.56	42.39 ± 0.59	42.89 ± 0.25	± 0.12
800	53.68	53.91 ± 0.33	54.07 ± 0.08	± 0.04

We can also study top-quark FB asymmetry at a more exclusive level, namely the FB asymmetry in different $|\cos\theta_t|$ bins, $A_{FB,bin}$. In Fig. 5, we plot ratios of the NLO and NNLO predictions on $A_{FB,bin}$ to the LO ones for $\sqrt{s} = 400$ GeV. Both the $\mathcal{O}(\alpha_s)$ and $\mathcal{O}(\alpha_s^2)$ corrections are almost flat on $|\cos\theta_t|$ for $\sqrt{s} = 400$ GeV. They decrease slightly with increasing $|\cos\theta_t|$ for $\sqrt{s} = 500$ GeV which is not shown here due to limited space.

Conclusions.—We have presented the first complete NNLO QCD corrections to top-quark pair production at e^+e^- collisions. The calculation is at fully differential level based on a generalization of the phase space slicing method to NNLO in QCD [7]. We have studied in detail the corrections to top-quark forward-backward asymmetry A_{FB}. The NNLO corrections to A_{FB} are half the size of the NLO corrections or even larger, for a typical collision energy of 400–500 GeV at future linear colliders. Moreover, our results show a large reduction of the theoretical uncertainties for predictions on A_{FB}. The residual scale uncertainty is well below the projected experimental precision. Our results allow for a precise determination of the top-quark neutral-current couplings at future linear colliders, which can be used to probe various new physics beyond the SM. Besides, there could be several interesting applications of the method and results presented here. First, it would be interesting to apply this calculation to charm- and bottom-quark production at Z boson mass pole. Second, decay of the Higgs boson to massive quarks can be calculated in a similar way to NNLO in QCD, since the two-loop matrix elements are available [28]. Third, it should be straightforward to combine production and leptonic decay [8,29] of top-quark pair in e^+e^- collisions within narrow-width approximation at NNLO. Last but not least, our calculation may also be

used to improve the accuracy of event shape resummation related to heavy-quark mass measurement [30].

We are grateful to Ye Li for careful reading and comments to the manuscript. This work was supported by the U.S. DOE under Contract No. DE-AC02-76SF00515, Early Career Research Award DE-SC0003870, by Lightner-Sams Foundation, and the Munich Institute for Astro- and Particle Physics (MIAPP) of the DFG Cluster of Excellence "Origin and Structure of the Universe." Work at ANL is supported in part by the U.S. Department of Energy under Contract No. DE-AC02-06CH11357. H. X. Z. thanks the theory group of Paul Scherrer Institute (PSI) at Zurich and the Center for Future High Energy Physics (CFHEP) at Beijing for hospitality where the project was finalized.

*jgao@anl.gov
†hxzhu@slac.stanford.edu

[1] H. Baer, T. Barklow, K. Fujii, Y. Gao, A. Hoang, S. Kanemura, J. List, H. E. Logan *et al.*, arXiv:1306.6352.

[2] A. Czarnecki and K. Melnikov, Phys. Rev. Lett. **80**, 2531 (1998); M. Beneke, A. Signer, and V. A. Smirnov, Phys. Rev. Lett. **80**, 2535 (1998); A. H. Hoang and T. Teubner, Phys. Rev. D **58**, 114023 (1998); M. Beneke, A. Signer, and V. A. Smirnov, Phys. Lett. B **454**, 137 (1999).

[3] M. Beneke, Y. Kiyo, P. Marquard, A. Penin, J. Piclum, D. Seidel, and M. Steinhauser, Phys. Rev. Lett. **112**, 151801 (2014).

[4] S. G. Gorishnii, A. L. Kataev, and S. A. Larin, Nuovo Cimento A **92**, 119 (1986); K. G. Chetyrkin and J. H. Kuhn, Phys. Lett. B **248**, 359 (1990); K. G. Chetyrkin and J. H. Kuhn, Nucl. Phys. **B432**, 337 (1994); R. Harlander and M. Steinhauser, Eur. Phys. J. C **2**, 151 (1998); K. G. Chetyrkin, R. Harlander, J. H. Kuhn, and M. Steinhauser, Nucl. Phys. **B503**, 339 (1997).

[5] W. Bernreuther, R. Bonciani, T. Gehrmann, R. Heinesch, T. Leineweber, P. Mastrolia, and E. Remiddi, Nucl. Phys. **B706**, 245 (2005); W. Bernreuther, R. Bonciani, T. Gehrmann, R. Heinesch, T. Leineweber, P. Mastrolia, and E. Remiddi, Nucl. Phys. **B712**, 229 (2005); W. Bernreuther, R. Bonciani, T. Gehrmann, R. Heinesch, T. Leineweber, and E. Remiddi, Nucl. Phys. **B723**, 91 (2005); J. Gluza, A. Mitov, S. Moch, and T. Riemann, J. High Energy Phys.. 07 (2009) 001.

[6] W. Bernreuther, A. Brandenburg, and P. Uwer, Phys. Rev. Lett. **79**, 189 (1997); G. Rodrigo, A. Santamaria, and M. S. Bilenky, Phys. Rev. Lett. **79**, 193 (1997); P. Nason and C. Oleari, Phys. Lett. B **407**, 57 (1997); A. Brandenburg and P. Uwer, Nucl. Phys. **B515**, 279 (1998); P. Nason and C. Oleari, Nucl. Phys. **B521**, 237 (1998); G. Rodrigo, M. S. Bilenky, and A. Santamaria, Nucl. Phys. **B554**, 257 (1999).

[7] J. Gao and H. X. Zhu, arXiv:1408.5150 [Phys. Rev. D (to be published)].

[8] J. Gao, C. S. Li, and H. X. Zhu, Phys. Rev. Lett. **110**, 042001 (2013).

[9] A. von Manteuffel, R. M. Schabinger, and H. X. Zhu, arXiv:1408.5134.

[10] A. Gehrmann-De Ridder, T. Gehrmann, and E. W. N. Glover, J. High Energy Phys. 09 (2005) 056; W. Bernreuther, C. Bogner, and O. Dekkers, J. High Energy Phys. 06 (2011) 032; G. Abelof and A. Gehrmann-De Ridder, J. High Energy Phys. 11 (2012) 074; G. Abelof, O. Dekkers, and A. Gehrmann-De Ridder, J. High Energy Phys. 12 (2012) 107; W. Bernreuther, C. Bogner, and O. Dekkers, J. High Energy Phys. 10 (2013) 161; G. Abelof, A. Gehrmann-De Ridder, P. Maierhofer, and S. Pozzorini, J. High Energy Phys. 08 (2014) 035; G. Abelof and A. G. D. Ridder, arXiv:1409.3148.

[11] O. Dekkers and W. Bernreuther, Phys. Lett. B **738**, 325 (2014).

[12] G. Altarelli and B. Lampe, Nucl. Phys. **B391**, 3 (1993); V. Ravindran and W. L. van Neerven, Phys. Lett. B **445**, 214 (1998); S. Catani and M. H. Seymour, J. High Energy Phys. 07 (1999) 023.

[13] W. Bernreuther, R. Bonciani, T. Gehrmann, R. Heinesch, T. Leineweber, P. Mastrolia, and E. Remiddi, Nucl. Phys. **B750**, 83 (2006).

[14] K. Agashe, R. Contino, and R. Sundrum, Phys. Rev. Lett. **95**, 171804 (2005); M. S. Carena, E. Ponton, J. Santiago, and C. E. M. Wagner, Nucl. Phys. **B759**, 202 (2006); R. Contino, T. Kramer, M. Son, and R. Sundrum, J. High Energy Phys. 05 (2007) 074.

[15] R. S. Chivukula, S. B. Selipsky, and E. H. Simmons, Phys. Rev. Lett. **69**, 575 (1992); R. S. Chivukula, E. H. Simmons, and J. Terning, Phys. Lett. B **331**, 383 (1994); A. Pomarol and J. Serra, Phys. Rev. D **78**, 074026 (2008).

[16] E. Devetak, A. Nomerotski, and M. Peskin, Phys. Rev. D **84**, 034029 (2011).

[17] M. S. Amjad, M. Boronat, T. Frisson, I. Garcia, R. Poschl, E. Ros, F. Richard, J. Rouene *et al.*, arXiv:1307.8102.

[18] M. S. Amjad, T. Frisson, E. Kou, R. Poschl, F. Richard, and J. Rouene, Nuovo Cimento C **037**, 55 (2014).

[19] S. Frixione, Z. Kunszt, and A. Signer, Nucl. Phys. **B467**, 399 (1996).

[20] S. Catani and M. H. Seymour, Nucl. Phys. **B485**, 291 (1997); **B510**, 503 (1998).

[21] G. Cullen, H. van Deurzen, N. Greiner, G. Heinrich, G. Luisoni, P. Mastrolia, E. Mirabella, G. Ossola *et al.*, arXiv:1404.7096.

[22] P. Mastrolia, E. Mirabella, and T. Peraro, J. High Energy Phys. 06 (2012) 095; 11 (2012) 128.

[23] T. Peraro, Comput. Phys. Commun. **185**, 2771 (2014).

[24] A. van Hameren, C. G. Papadopoulos, and R. Pittau, J. High Energy Phys. 09 (2009) 106.

[25] A. van Hameren, Comput. Phys. Commun. **182**, 2427 (2011).

[26] A. Denner and T. Sack, Nucl. Phys. **B358**, 46 (1991).

[27] J. Beringer *et al.* (Particle Data Group), Phys. Rev. D **86**, 010001 (2012).

[28] W. Bernreuther, R. Bonciani, T. Gehrmann, R. Heinesch, P. Mastrolia, and E. Remiddi, Phys. Rev. D **72**, 096002 (2005).

[29] M. Brucherseifer, F. Caola, and K. Melnikov, J. High Energy Phys. 04 (2013) 059.

[30] S. Fleming, A. H. Hoang, S. Mantry, and I. W. Stewart, Phys. Rev. D **77**, 074010 (2008).